Mathematics Scientific Journal

Vol. 7, No. 1, (2011), 21-62

Modeling, simulation and analysis of a multi degree of freedom aircraft wing model

Xueguang Bi[a,1], Yucheng Liu[b,2]

[a] ***Stanley Security Solutions, Inc., Shenzhen, Guangdong 518108, China;***

[b] ***Department of Mechanical Engineering, University of Louisiana, Lafayette, LA 70504, USA;***

Received 1 January 2010; Accepted 17 October 2010

Abstract

This paper presented methods to determine the aerodynamic forces that act on an aircraft wing during flight. These methods are initially proposed for a simplified two degree-of-freedoms airfoil model and then are extensively applied for a multi-degree-of-freedom airfoil system. Different airspeed conditions are considered in establishing such methods. The accuracy of the presented methods is verified by comparing the estimated aerodynamic forces with the actual values. A good agreement is achieved through the comparisons and it is verified that the present methods can be used to correctly identify the aerodynamic forces acting on the aircraft wing models.

***Keywords*:** Freedom system, Force Determination Methods, Aircraft wing model

[2] **Corresponding Author's E-mail: yucheng.liu@louisiana.edu**

1. Introduction

During flight, aircraft wings always subject to varying aerodynamic loadings and as a consequence, generate varying structural responses. The varying aerodynamic loadings and structural responses are coupled to create a complicated vibration effect known as structural coupling dynamics. This effect can significantly reduce the aircraft's service life. Even worse, sometimes the sustained vibration at natural frequencies of airfoils may lead to catastrophic structural failure.

Recently, a number of researchers have dedicated tremendous effort to developing and choosing light material for the aircraft in order to obtain effective loading capacity. However, as the aircraft speed continues to increase, its structural flexibility is becoming a dominant concern in aircraft design and causing serious flutter in the airfoil and other components.

Considering a typical cross-sectional plane of an airfoil, the gravity center G is usually located at 42% ~ 45% of the chord line, and the elasticity center is located at 38% ~ 40% of the chord line (Fig. 1). The gravity center is not coincident with the elastic center, which results in another coupling effect between the translational and rotational degree-of-freedoms of the aircraft wing. This coupling effect and the aforementioned structural coupling dynamics make it too difficult to correctly determine the aerodynamic forces acting on the aircraft wings.

The current methods of studying the dynamic response of the aircraft structure consider the structural model and the aerodynamic model separately and therefore fails to precisely simulate the two coupling effects. In this paper, new methods are presented to determine the aerodynamic forces acting on aircraft wings during flight, which considers the model's structural elasticity and

aerodynamics as a combined mathematical system. The methods are initiated based on a simplified two degree-of-freedoms airfoil system and then they will be applied for a finite element aircraft wing model, which is a multi-degree-of-freedom system. The accuracy of the present methods will be verified by comparing the estimated aerodynamic forces with the actual values.

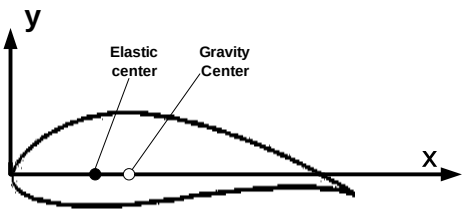

Figure 1. The schematic diagram for the centers of an airfoil

2. Literature Review

Dynamic response of aircraft model during flight has received a lot of interests, and a number of methods have been developed about the simulating and analyzing the aircraft structures.

Yosibash and Kirby [1] constructed a high order simulation model of fluid-structure for the airfoil under flying conditions. The authors utilized spectral/hp solver for fluid (air) and hp-FEM solver for the airfoil to handle the coupling problem generated by aerodynamic and structure interaction. The two solvers somehow can minimize the modeling errors and the discretization errors. The ongoing verification and validation of fluid-structure interaction are also presented. In their study the airfoil was treated as a flexible thin plate in the flow and the one-way coupling and two-way coupling were discussed separately. The

coupled fluid-structure method was also used by Liu et al [2] in calculation of wing flutter. Fabunmi [3] presented a method of using the pseudo-inverse technique to determine the operating vibratory loads on a structural system. In his work, two types of uniform beam were studied: the cantilever beam and the free end beam. Results of numerical calculations showed that the accuracy of the determined forces correlates well with a parameter that is related to the number of modes contributing to the response of the structure at a given frequency. Shyy and Kamakoti [4] studied the interactions between rigid and flexible structures and fluid based on an airfoil system model. A loosely coupled approach was used to perform the combined fluid and structure computations. Two different airfoil configurations were employed to obtain the displacement of the airfoil and the pressure on it. A suitable interfacing technique was incorporated to couple and synchronize the flow and structure solver. Liu and Shepard [5] addressed an approach of dynamic force identification based on enhanced least squares and total least-squares schemes in the frequency domain. This approach is effective in reducing the random errors that occur in structural response signals. Two regularization filters, named as the truncated singular value decomposition (TSVD) filter and the Tikhonov filter, were employed in conjunction with the conventional least-squares scheme at specific frequencies. A new least-squares form of the Morozov's discrepancy principle was formulated to aid in selecting the optimum regularization parameter for these filters at each frequency. The accuracy in using conventional least-squares, TSVD-based least-squares, and Tikhonov filter-based least-squares schemes were compared analytically and numerically in their study. E. Parloo et al [6] demonstrated a method of identifying dynamic force by means of in-operation modal models. The applicability of the sensitivity-based normalization approach for force identification on the basis of output-only data was evaluated. The quality of the reconstructed FRF data and the advantages of using an iterative weighted pseudo-inverse approach over a classic pseudo-inverse one were discussed through experiments performed on a beam structure.

Aerodynamics of airfoil models remains an important topic in aircraft research, and most recent work in the area involves some aspect of airfoil modeling and its nonlinear aeroelastic analysis. Kim and Lee [7,8] created a two-dimensional flexible airfoil with a freeplay nonlinearity in pitch and analyzed this model in the subsonic flow range. Structurally, the airfoil was modeled as finite beam elements and two spring elements in pitch and plunge. A doublet lattice method was used for the two-dimensional unsteady aerodynamics to include the camber deflection effect. The fictitious mass modal approach was adopted in order to use the consistent modal coordinates for the structures with nonlinearity. Nonlinear aeroelastic analyses for both the frequency domain and time domain were performed for rigid and flexible airfoil models to investigate the flexibility effect. Dynamic response of this airfoil model such as limit cycle oscillation and chaotic motion were observed and they were highly influenced by the pitch-to-plunge frequency ratio. Lee et al [9] derived the equations of motion of a two-dimensional airfoil oscillating in pitch and plunge for a structural nonlinearity using subsonic aerodynamic theory. In their works, three classical aerodynamic nonlinearities involving cubic, freeplay and hysteresis were investigated in detail.

Besides the simplified two-dimensional models, more complicated aircraft wing models were created for purpose of analytical analysis, which usually are multi-degree-of-freedom models. Roy and Eversman [10,11] created a multi-degree-of-freedom finite element model for the flexile wing structure, with beam elements for bending and rod elements for torsion. This model was then used to investigate the potential of an adaptive feed-forward controller for active flutter suppression of a flexible wing. Dimitriadis and Cooper [12] presented a method for identification of non-linear multi-degree-of-freedom systems and used this method to model aeroelastic systems for tracking the stability of aircraft during flight flutter testing.

3. Two Degree-of-Freedoms System

The aircraft wing, which is modeled as a two degree-of-freedoms pitch-plunge system (Fig. 2), is governed by the following equations of motion:

$$M\ddot{x} + (C + UL)\dot{x} + (K + U^2 H)x = bf_a \tag{1}$$

Here

$$x = \begin{bmatrix} x \\ \theta \end{bmatrix}, b = \begin{bmatrix} 1 \\ -c_a \end{bmatrix}, M = \begin{bmatrix} m & 0 \\ 0 & I \end{bmatrix}, C = \alpha K, K = \begin{bmatrix} k & -ke \\ -ke & k_\theta + ke^2 \end{bmatrix}, H = \frac{\rho c}{2}\frac{dC_L}{d\theta}\begin{bmatrix} 0 & 1 \\ 0 & c\left(\frac{1}{4} - \frac{c_0}{c}\right) \end{bmatrix},$$

$$L = \frac{\rho c}{2}\frac{dC_L}{d\theta}\begin{bmatrix} 1 & c\left(\frac{3}{4} - \frac{c_0}{c}\right) \\ c\left(\frac{1}{4} - \frac{c_0}{c}\right) & c^2\left(\frac{1}{4} - \frac{c_0}{c}\right)\left(\frac{3}{4} - \frac{c_0}{c}\right) + \left(\frac{8}{\pi}\right)\Big/\left(\frac{dC_L}{d\theta}\right) \end{bmatrix} \tag{2}$$

where m and I are mass and mass moment of inertia about the gravity center, respectively; f_a is the excitation force from the aileron; α is the proportional damping constant; k and k_θ are translational and rotational structural stiffness, respectively, e is the distance between the gravity and the elastic center; U denotes air speed; ρ denotes air density; c denotes chord length; c_0 is the distance between the leading edge and the elastic center; and C_L is the local lift coefficient. The derivative $dC_L/d\theta$ is assumed to be constant, with a theoretical value of 2π for incompressible flow.

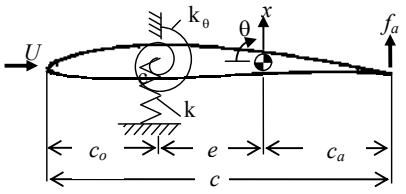

Figure 2. The two degree freedom system for airfoil

Rewrite Eqn. (1) into the state space form and we have:

$$\dot{Y} = AY + Bf_a \tag{3}$$

Here

$$Y = [x, \dot{x}, \theta, \dot{\theta}]^T, A = \begin{bmatrix} 0 & I \\ -M^{-1}(K + U^2 H) & -M^{-1}(C + UL) \end{bmatrix}, B = [0, M^{-1}]^T \tag{4}$$

where A and B are the system and input matrices, respectively. The system states then can be determined from Eqn. (3) in the frequency domain as:

$$Y(\omega) = (j\omega I - A)^{-1} B F_a(\omega) \tag{5}$$

The eigenvalues λ_i of the system matrix A are functions of the air speed U, which are related to the system's natural frequencies ω_{ni} and damping ratios ζ_i as:

$$\lambda_i = -\zeta_i \omega_{ni} \pm j\omega_{ni}\sqrt{1-\zeta_i^2} \tag{6}$$

As shown in Fig. 3a, when U increases, ω_{n1} increases and ω_{n2} decreases steadily. The damping ratio of the second mode ζ_2 decreases with an increasing airspeed U and it reaches zero at the critical speed U_{cr}. At air speed $U > U_{cr}$, $\zeta_2 < 0$, and hence the system becomes unstable.

In the time domain, the equations of the motion for the system (Fig. 2) can be written as:

$$M\ddot{x} + C\dot{x} + Kx = bf_a - UL\dot{x} - U^2 Hx; \tag{7}$$

where, on the right hand side are the aerodynamic force and the excitation force at the aileron, which are referred to actual forces on the system. The objective of this study is to determine the actual forces using the displacement data measured during the aircraft's flight.

Indirect force identification is a method for estimating dynamic forces acting on a structural or mechanical system by using the system's frequency response matrix and response measurements. This method is often used to determine the unknown dynamic forces that occur when the system is operating, at which time these forces cannot be directly measured. This method is derived from the multi-input/multi-output (MIMO) transfer function relationship for linear systems as:

$$X(\omega) = H(\omega) \cdot F(\omega) \tag{8}$$

where ω is frequency; X(ω) is an output vector of the system's structural responses; F(ω) is an input vector of applied dynamic forces; and H(ω) is the frequency response matrix of this system. Assuming H(ω) is known, and the F(ω) can be determined as:

$$F(\omega) = H(\omega)^{-1} \cdot X(\omega) \text{ (H(ω) is a square matrix)} \tag{9}$$

or

$$F(\omega) = [H(\omega)^T H(\omega)]^{-1} H(\omega)^T \cdot X(\omega) \text{ (H(ω) is a non-square matrix)} \tag{10}$$

From above equations, it can be seen that in order to determine the force F(ω), the H(ω) and X(ω) has to be constructed or measured through experiments.

The objective of this study is to identify the distributed aerodynamic force and moment acting on an aircraft wing during the flight. By employing the indirect force identification for this problem, the wing's frequency response matrix H(ω) has to be obtained from a ground vibration test (GVT), where both the excitation and response are measurable. Next, the output structural response X(ω) is measured and the F(ω) can then be calculated from Eqn. (9) or (10). Different force determination methods used in this study are demonstrated in following sections.

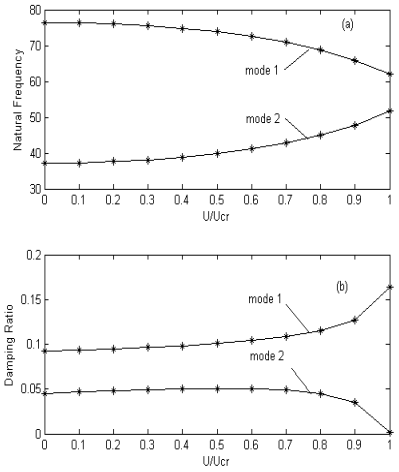

Figure 3. (a) Natural frequencies, (b) damping ratios as a function of airspeed**.**

4. Force Determination Methods

4.1 Traditional force determination method

Instead of measuring the H(ω) experimentally, the frequency response matrix can also be found from the equation:

$$H(\omega) = (-\omega^2 M + j\omega C + K)^{-1} \tag{11}$$

In Eqn. (11), noise can be directly added to H(ω) in order to represent an experimentally measured frequency response matrix which involves the noise effects. According to Fabunmi [3], we have:

$$H(\omega) = H(\omega) + E_{noise}, \text{ and } E_{noise} = \gamma \frac{\left| \sum_{i,j=1}^{p} H_{ij}(\omega) \right|}{p} \rho \tag{12}$$

Here γ is the percentage error level and ρ is a randomly generated number which belongs to [-1, 1]. The frequency response matrix H(ω) then can be inverted and used in Eqn. (8) to identify the external forces F(ω).

4.2 Force determination using "H_1"& "H_2" estimated frequency response matrices

As an alternative approach, consider that H(ω) can be determined from experimental data measured through conducting a ground vibration test on an aircraft. In order to simulate the experiment, random measurement noise is added to the force and displacement signals.

$$F(\omega) = F(\omega) + N_f, \text{ and } N_f = \left| \sum_{i=1}^{100} F(\omega) \right| \gamma\rho \tag{13}$$

$$X(\omega) = X(\omega) + N_x, \text{ and } N_x = \left|\sum_{i=1}^{100} X(\omega)\right|\gamma\rho \tag{14}$$

where γ is the noise level. The frequency response matrix then can be estimated from the measured data by [6]:

$$H_1 = G_{FX}G_{FF}^{-1} \tag{15}$$

$$H_2 = G_{XX}G_{XF}^{-1} \tag{16}$$

Here "H_1" and "H_2" are the estimated frequency response matrices, G_{FF} and G_{FX} are auto-power spectrum of force (F) and cross-power spectrum of force (F) and displacement (X), respectively. Likewise, G_{XX} and G_{XF} are auto-power spectrum of displacement (X) and cross-power spectrum of displacement (X) and force (F). The frequency response matrices determined by Eqn. (15) or (16) are transposed and inverted, and then are substituted into Eqn. (9) or (10) to calculate the forces F(ω). Such method is called "H_1" and "H_2" force determination method.

4.3 Direct force determination "F_1" and "F_2" methods

The "H_1" and "H_2" force estimation methods can be improved by following transformation, from Eqn. (15) we have:

$$H_1^{-1} = G_{FF}G_{FX}^{-1},\ H_1^{T} = G_{FF}^{-T}G_{FX}^{T},\ and\ H_1^{-T} = G_{FX}^{-T}G_{FF}^{T} \tag{17}$$

Similarly, from Eqn. (16) we have:

$$H_2^{-1} = G_{XF}G_{XX}^{-1},\ H_1^{T} = G_{XF}^{-T}G_{XX}^{T},\ and\ H_1^{-T} = G_{XX}^{-T}G_{XF}^{T} \tag{18}$$

Eqns. (17) and (18) calculate the inverted frequency response matrix directly, which can reduce the error introduced during the inversion of the frequency response matrix. The forces then can be calculated by substituting Eqns. (17),

(18) into Eqn. (9) or (10).

5. Validation of Force Determination Methods – Two Degrees-of-Freedom Model

To verify the aforementioned force determination approaches, these methods are employed to simulate the two degree-of-freedoms airfoil system model (Figs. 1 and 2). At first, the traditional pseudo-inverse technique is employed to determine the aerodynamic forces and it is assumed that the frequency response function matrix for force determination is measured from experimental test. Fig. 4 plots the estimated Frequency Response Function H(ω) (FRF) using the traditional pseudo-inverse method, where H_{11} is the very first response function in the force response matrix [H]. The actual and estimated force and moment, as well as the percentage errors are also displayed in Figs. 5 and 6. As shown from these figures, by using the pseudo-inverse method, the percentage errors of the estimated force and moment are very low; with average values at 0.085% and 0.047%, respectively.

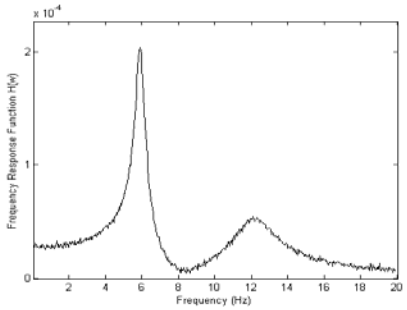

Figure 4. FRF H_{11} at U/Ucr = 0 with 5% noise using traditional inverse method, based on two degrees-of-freedom model.

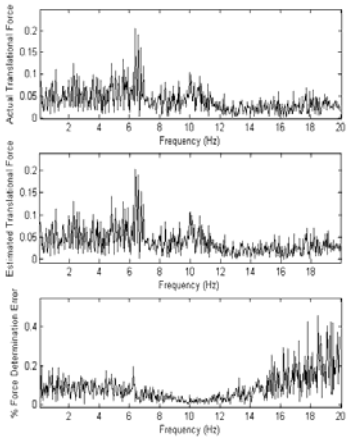

Figure 5. Actual, estimated, translational force and percentage error, U/Ucr = 2/3 with 5% noise using traditional inverse technique, based on two degrees-of-freedom model.

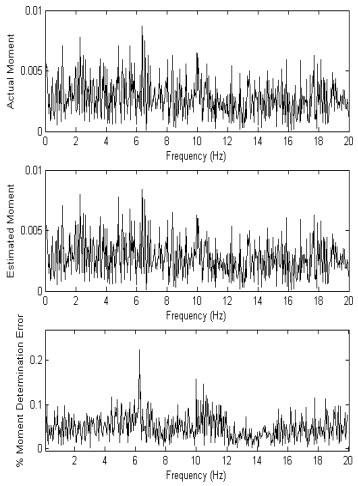

Figure 6. Actual, estimated rotational moment and percentage error, U/Ucr = 2/3 with 5% noise using traditional inverse technique, based on two degrees-of-freedom model.

Secondly, the frequency response function, actual and estimated forces and moments, as well as percentage errors are re-calculated by using "H_1" and "H_2" force determination methods. The sample rate to calculate H_1 and H_2 is 20 Hz, and the period is 0.05 seconds. Because the excitation force and noise added in this study are the random numbers, the simulation results will be slightly different each time the calculation is performed. Thus, we have to redo the calculation for a certain amount of times to obtain the average values of the results and use those values to compare and validate the different force determinations. In this study, the calculation is repeated 100 times so that the obtained average results are stable and predictable.

Figs. 7 to 9 display the FRF, actual and estimated force and displacement, and percentage errors obtained from the H_1 method. Figs. 10 to 12 depict the same results obtained from the H_2 method. Here the noise is added through the method described in Eqns. (13) and (14). The results are formulated at air speed of 7.666 m/s and 5% noise level. As shown in Figs. 8 and 9, the average percentage errors for the force and moment obtained from the H_1 method are 6.24% and 7.61%, respectively. Nevertheless, from Figs.11 and 12, the average percentage errors for the force and moment yielded from the H_2 method are 31.41% and 25.35%.

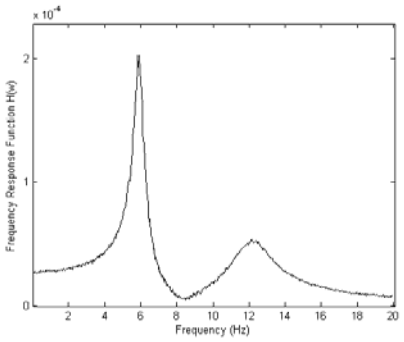

Figure 7. FRF H_{11} at U/Ucr = 0 with 5% noise using H_1 method, based on two degrees-of-freedom model.

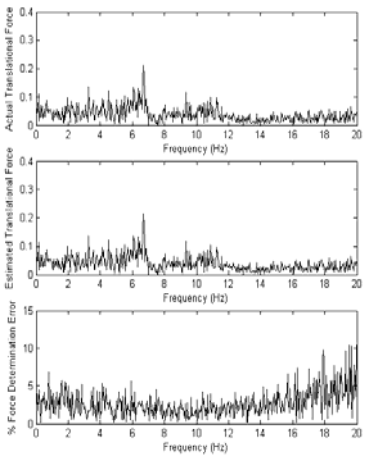

Figure 8. Actual, estimated translational force and percentage error, U/Ucr = 2/3 with 5% noise using H_1 method, based on two degrees-of-freedom model.

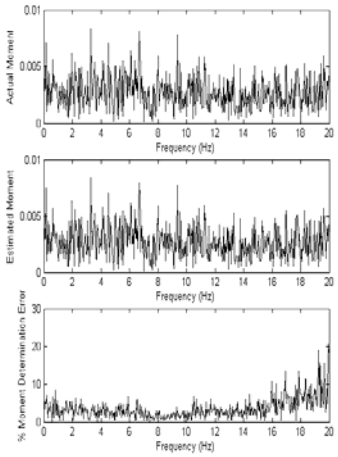

Figure 9. Actual, estimated rotational moment and percentage error, U/Ucr = 2/3 with 5% noise using H_1 method, based on two degrees-of-freedom model.

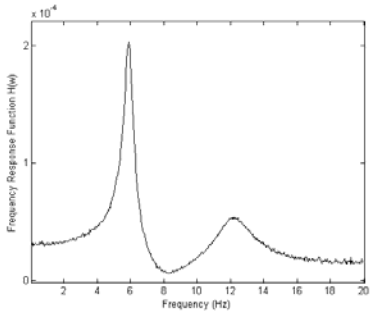

Figure 10. FRF H_{11} at U/Ucr = 0 with 5% noise using H_2 method, based on two degrees-of-freedom model.

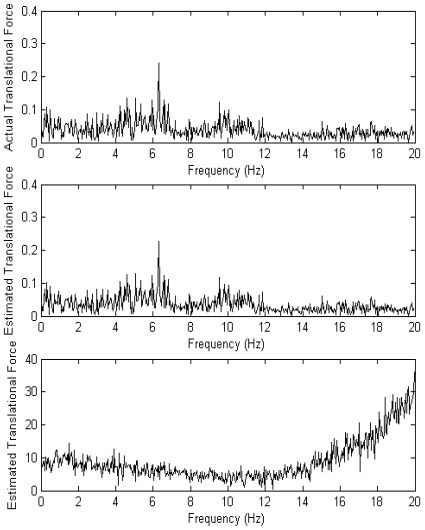

Figure11. Actual, estimated translational force and percentage error, U/Ucr = 2/3 with 5% noise using H_2 method, based on two degrees-of-freedom model.

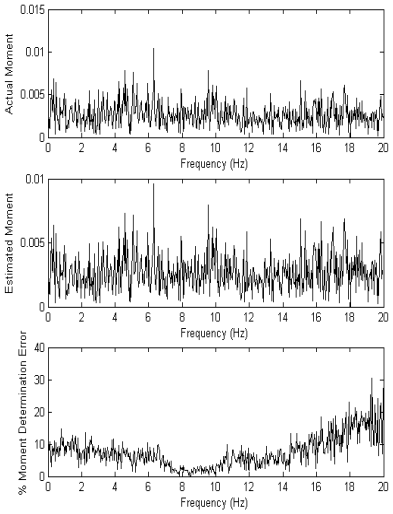

Figure12. Actual, estimated rotational moment and percentage error, U/Ucr = 2/3 with 5% noise using H_2 method, based on two degrees-of-freedom model.

Finally, actual, estimated forces and moments, and the percentage errors are recalculated using the "F_1" and "F_2" methods and plotted in Figs. 13 to 16. The displayed results are obtained at the airspeed of 7.666 m/s and noise level of 5%. Based on Figs. (13) and (14), the average percentage errors for the force and moment yielded from the "F_1" method are 2.69% and 0.47%, while these values are 8.90% and 0.47% given by the "F_2" method, according to the Figs. (15) and (16).

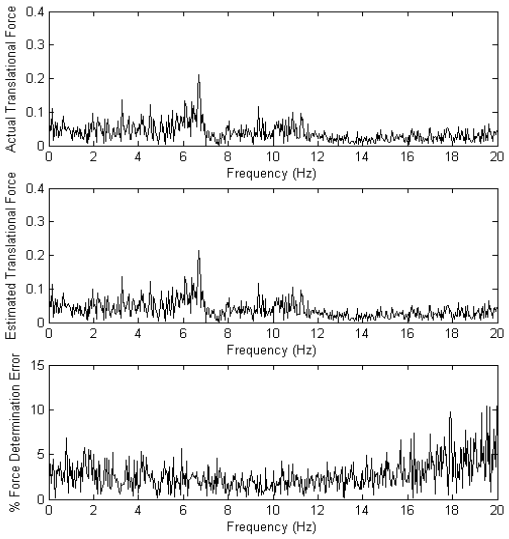

Figure 13. Actual, estimated translational force and percentage error, U/Ucr = 2/3 with 5% noise using F_1 method, , based on two degrees-of-freedom model.

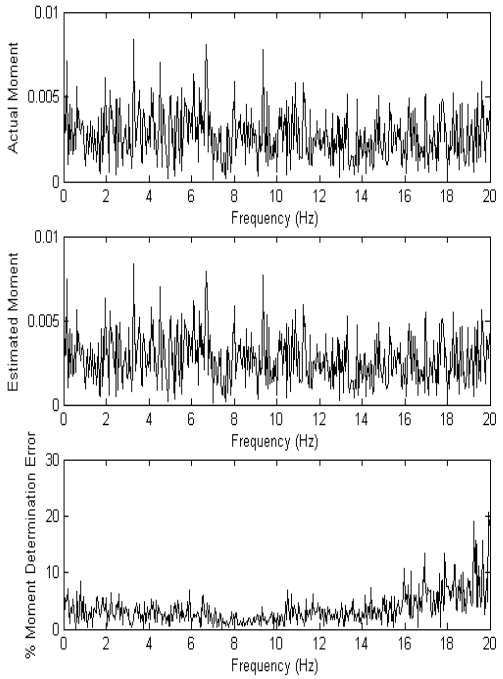

Figure14. Actual, estimated rotational moment and percentage error, U/Ucr = 2/3 with 5% noise using F_1 method, based on two degrees-of-freedom model.

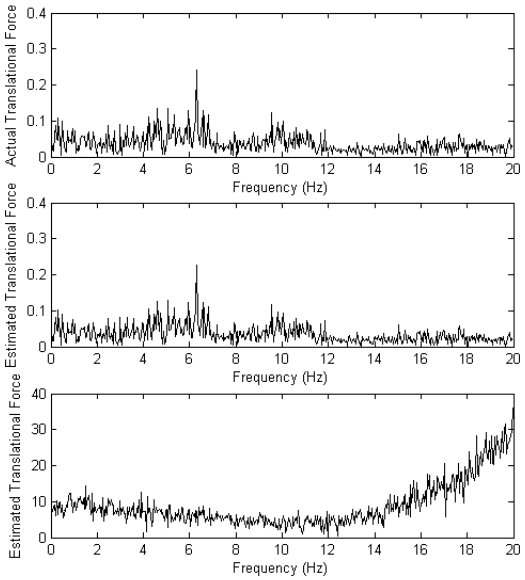

Figure15. Actual, estimated translational force and percentage error, U/Ucr = 2/3 with 5% noise using F_2 method, based on two degrees-of-freedom model.

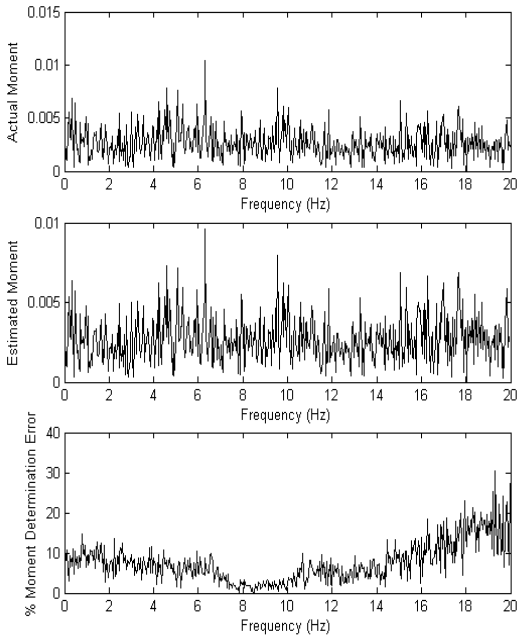

Figure16. Actual, estimated rotational moment and percentage error, U/Ucr = 2/3 with 5% noise using F_2 method, based on two degrees-of-freedom model.

6. Multi Degree-of-Freedom Aircraft Wing Model

The presented force determination methods (Eqns. (9) to (18)) are then applied for multi-degree-of-freedom wing models.

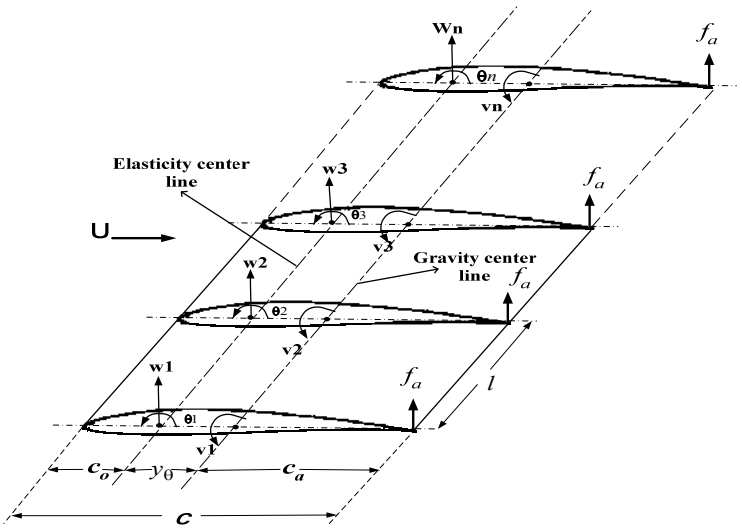

Figure 17. Finite element aeroelastic aircraft wing model

As shown in Fig. 17, an aircraft wing is modeled as a multi-degree-of-freedom pitch-plunge system with torsional and bending beam elements. This system is also governed by Eqn. (1), where M and K are mass and stiffness matrices for the beam elements. For each beam element "i", its mass and stiffness matrices are:

$$M_i = \begin{bmatrix} 2a & a & 156by_\theta & 0 & 54by_\theta & 0 \\ a & 2a & 54by_\theta & 0 & 156by_\theta & 0 \\ 156by_\theta & 54by_\theta & 156b & 22lb & 54b & -13lb \\ 0 & 0 & 22lb & 4l^2b & 13lb & -3l^2b \\ 54by_\theta & 156by_\theta & 54b & 13lb & 156b & -22lb \\ 0 & 0 & -13lb & -3l^2b & -22lb & 4l^2b \end{bmatrix} \tag{19}$$

$$K_i = \begin{bmatrix} c & -c & 0 & 0 & 0 & 0 \\ -c & c & 0 & 0 & 0 & 0 \\ 0 & 0 & 12d & 6ld & -12d & 6ld \\ 0 & 0 & 6ld & 4l^2d & -6ld & 2l^2d \\ 0 & 0 & -12d & -6lb & 12d & -6ld \\ 0 & 0 & 6ld & 2l^2d & -6lb & 4l^2d \end{bmatrix} \quad (20)$$

Here a = (ρI_pl)/6, b = (ρAl)/420, c = GJ/l, d = EI/l^3, y_θ is the Y-distance between the wing's gravity and elastic center; ρ is the material's density; I_p and I are the polar and regular moment of inertia of the wing model's cross section, respectively; A is the cross-sectional area; l denotes the length of single element; G denotes the shear modulus of elasticity; J represents the polar moment of inertia; and E is the Young's modulus (see Fig. 17). The input vector b and the proportional damping matrix C are given as:

$$b = [-c_a, -c_a, \ldots, -c_a, 1, 1, \ldots, 1]; C = \alpha M + \beta K \quad (21)$$

where c_a is the Y-distance between the trailing edge and the gravity center, and α and β are the proportional damping constant.

The displacement vector x (assume this model has n elements):

$$x = [\theta, x]^T = [\theta_1, \ldots, \theta_n, x_1, \ldots, x_n]^T \quad (22)$$

where θ_i is the i^{th} element's rotational displacement and x_i is its translational displacement. The system's mass and stiffness matrices can be written as:

$$M=\left[\begin{array}{cccc:cccccc}
2a & a & 0 & \cdots & 156by_\theta & 0 & 54by_\theta & 0 & 0 & 0 & \cdots \\
a & 4a & a & \cdots & 54by_\theta & 0 & 312by_\theta & 0 & 54by_\theta & 0 & \cdots \\
0 & a & 4a & \cdots & 0 & 0 & 54by_\theta & 0 & 312by_\theta & 0 & \cdots \\
\vdots & \vdots & \vdots & \vdots & \vdots & \vdots & \vdots & \vdots & \vdots & \vdots & \vdots \\
\hdashline
156by_\theta & 54by_\theta & 0 & \cdots & 156b & 22lb & 54b & -13b & 0 & 0 & \cdots \\
0 & 0 & 0 & \cdots & 22lb & 4l^2b & 13lb & -3l^2b & 0 & 0 & \cdots \\
54by_\theta & 312by_\theta & 54by_\theta & \cdots & 54lb & 13lb & 312b & 0 & 54b & -13lb & \cdots \\
0 & 0 & 0 & \cdots & -13lb & -3l^2b & 0 & 8l^2b & 13lb & -3l^2b & \cdots \\
0 & 54by_\theta & 312by_\theta & \cdots & 0 & 0 & 54b & 13lb & 312b & 0 & \cdots \\
0 & 0 & 0 & \cdots & 0 & 0 & -13lb & -3l^2b & 0 & 8l^2b & \cdots \\
\vdots & \vdots & \vdots & \vdots & \vdots & \vdots & \vdots & \vdots & \vdots & \vdots & \vdots
\end{array}\right]$$

(23)

$$K=\left[\begin{array}{cccc:cccccc}
c & -c & 0 & \cdots & 0 & 0 & 0 & 0 & 0 & 0 & \cdots \\
-c & 2c & -c & \cdots & 0 & 0 & 0 & 0 & 0 & 0 & \cdots \\
0 & -c & 2c & \cdots & 0 & 0 & 0 & 0 & 0 & 0 & \cdots \\
\vdots & \vdots & \vdots & \vdots & \vdots & \vdots & \vdots & \vdots & \vdots & \vdots & \vdots \\
\hdashline
0 & 0 & 0 & \cdots & 12d & 6ld & -12d & 6ld & 0 & 0 & \cdots \\
0 & 0 & 0 & \cdots & 6lb & 4l^2d & -6ld & 2l^2d & 0 & 0 & \cdots \\
0 & 0 & 0 & \cdots & -12d & -6ld & 24d & 0 & -12d & 6ld & \cdots \\
0 & 0 & 0 & \cdots & 6ld & 2l^2d & 0 & 8l^2d & -6ld & 2l^2d & \cdots \\
0 & 0 & 0 & \cdots & 0 & 0 & -12d & -6ld & 24b & 0 & \cdots \\
0 & 0 & 0 & \cdots & 0 & 0 & 6lb & 2l^2d & 0 & 8l^2d & \cdots \\
\vdots & \vdots & \vdots & \vdots & \vdots & \vdots & \vdots & \vdots & \vdots & \vdots & \vdots
\end{array}\right]$$

(24)

H and L in Eqn. (1) for the multi-degree-of-freedom model are aerodynamic stiffness matrix and aerodynamic damping matrix, respectively, which are defined as:

$$H = \frac{\rho_0 c}{2}\frac{dC_L}{d\theta}\begin{bmatrix} 0 & 1 & 0 & \cdots \\ 0 & c(\frac{1}{4}-\frac{c_0}{c}) & 1 & \cdots \\ 0 & 0 & c(\frac{1}{4}-\frac{c_0}{c}) & \cdots \\ \vdots & \vdots & \vdots & \vdots \end{bmatrix} \tag{25}$$

$$L = \frac{\rho_0 c}{2}\frac{dC_L}{d\theta}\begin{bmatrix} 1 & c(\frac{3}{4}-\frac{c_0}{c}) & 0 & \cdots \\ c(\frac{1}{4}-\frac{c_0}{c}) & c^2[(\frac{1}{4}-\frac{c_0}{c})(\frac{3}{4}-\frac{c_0}{c})+\frac{8}{\pi}\Big/\frac{dC_L}{d\theta}+1 & c(\frac{3}{4}-\frac{c_0}{c}) & \cdots \\ 0 & c(\frac{1}{4}-\frac{c_0}{c}) & c^2[(\frac{1}{4}-\frac{c_0}{c})(\frac{3}{4}-\frac{c_0}{c})+\frac{8}{\pi}\Big/\frac{dC_L}{d\theta}+1 & \cdots \\ \vdots & \vdots & \vdots & \vdots \end{bmatrix} \tag{26}$$

where ρ_0 is the air density; c is the chord length, c_0 is the Y-distance between the leading edge and the elastic center (Fig. 17); and C_L is the local lift coefficient. The derivative $dC_L/d\theta$ is assumed to be constant, with a theoretical value of 2π for incompressible flow.

Boundary conditions are added on the global system, which assume that the initial bending, torsional, and translational displacements are zero. Similarly, for this multi-degree-of-freedom system, the governing equation (1) is rewritten in to the sate space form as Eqns. (3) and (4). At this time the "Y" in Eqn. (3) is represented as:

$$Y = [\theta_1,...,\theta_n, x_1,...,x_n, \dot{\theta}_1,...,\dot{\theta}_n, \dot{x}_1,...,\dot{x}_n]^T \tag{27}$$

Eqns. (5) and (6) are still applicable in calculating this multi-degree-of-freedom system's states in the frequency domain and the eigenvalues of the system matrix A.

Fig. 18 depicts the relationship between the natural frequencies and the airspeed, and Fig. 19 displays the relationship between the damping ratios and the airspeed. From those figures, it can be found that as the airspeed U increases, the damping ratio of the first mode ζ_2 decreases and becomes zero at the critical speed U_{cr}. At air speed $U > U_{cr}$, $\zeta_2 < 0$, and hence the system becomes unstable. The same phenomenon was observed from the two degrees-of-freedom system.

The first and second mode shapes of the aircraft wing model at the airspeed U = 0 are plotted in Figs. 20 and 21, where the first mode shape refers to bending and the second mode shape refers to torsion. Table 1 and 2 list the relationships between natural frequencies and damping rations and the airspeed (including the first six modes).

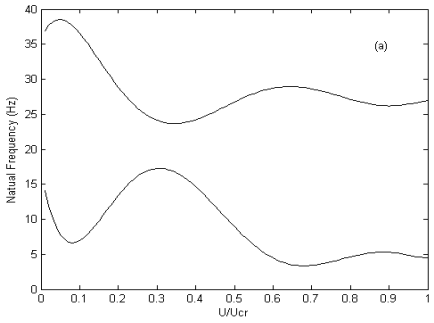

Figure 18. Natural frequencies vs. airspeed

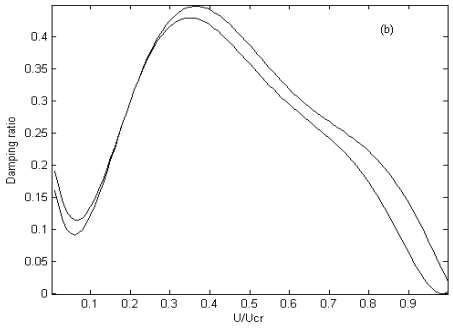

Figure 19. Damping ratios vs. airspeed

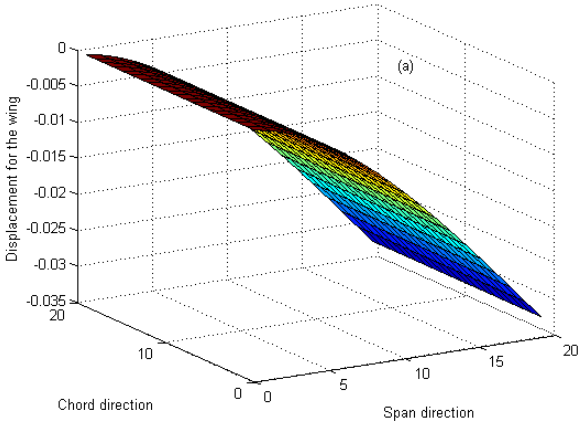

Figure 20. First mode shape at ω_1 = 16.244 Hz and U/Ucr = 0

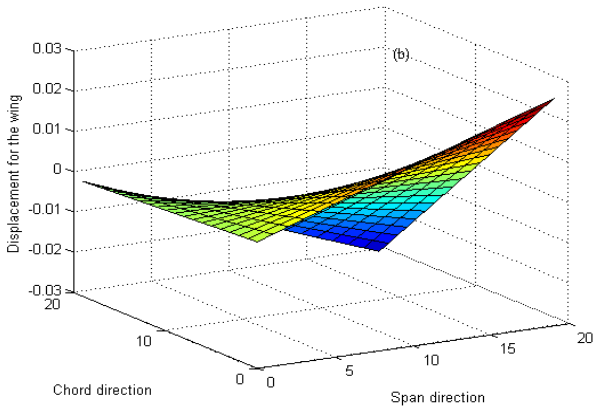

Figure 21. Second mode shape at ω_2 = 36.473 Hz and U/Ucr = 0

Table 1. Natural frequencies (Hz) vs. airspeed (U/U_{cr})

U/U_{cr}	Mode 1	Mode 2	Mode 3	Mode 4	Mode 5	Mode 6
0	16.244	36.473	160.55	500.55	1033.2	1759.5
0.1	10.382	33.6	166.24	251.95	458.47	973.09
0.2	6.8443	34.064	75.398	76.655	77.911	79.168
0.3	21.562	21.812	63.354	75.398	76.655	77.911
0.4	16.952	20.377	71.539	75.398	76.655	77.911
0.5	4.906	31.179	81.372	133.09	284.56	722.06
0.6	4.7606	28.554	79.008	122.5	253.82	625.86
0.7	4.7012	27.346	80.797	105.5	229.52	549.58
0.8	4.6794	26.908	82.433	91.309	210.22	489.76
0.9	4.676	26.879	68.724	98.201	193.98	442.13
1	4.6819	26.788	62.333	100.17	179.66	403.43

Table 2. Damping ratios vs. airspeed (U/U_{cr})

U/U_{cr}	Mode 1	Mode 2	Mode 3	Mode 4	Mode 5	Mode 6
0	0.19876	0.23049	0.24918	0.30178	0.40083	0.47871
0.1	0.10773	0.11821	0.17493	0.1767	0.26788	0.39319
0.2	0.32367	0.32681	0.38013	0.40906	0.48424	0.58842
0.3	0.40844	0.41564	0.43326	0.4727	0.52556	0.59122
0.4	0.40034	0.43584	0.45864	0.50383	0.54092	0.6478
0.5	0.37023	0.37241	0.46516	0.48108	0.62537	0.731
0.6	0.30117	0.34676	0.3704	0.51534	0.53147	0.75383
0.7	0.23902	0.26696	0.34486	0.41992	0.56749	0.65837
0.8	0.16434	0.19748	0.29465	0.36687	0.54666	0.63189
0.9	0.071974	0.1587	0.18241	0.40808	0.41975	0.70132
1	0.00014979	0.014406	0.19345	0.27838	0.46157	0.65677

7. Validation of Force Determination Methods – Two Degrees-of-Freedom Model

In this section, Eqns. (9) to (18) are applied to determine the aerodynamic forces acting on this multi-degree-freedom airfoil system and the estimated forces and moments are compared to the actual values.

First, the traditional pseudo-inverse technique is employed to determine the aerodynamic forces and the frequency response function matrix $H(\omega)$ is calculated from Eqns. (11) and (12). Fig. 22 displays the first response function in the force response matrix, H_{11}. Figs. 23 and 24 compare the actual and estimated forces and moments. From both figures, it can be found that by using the traditional pseudo-inverse method, the average percentages for the forces and moments are 0.2027% and 0.5962%, respectively.

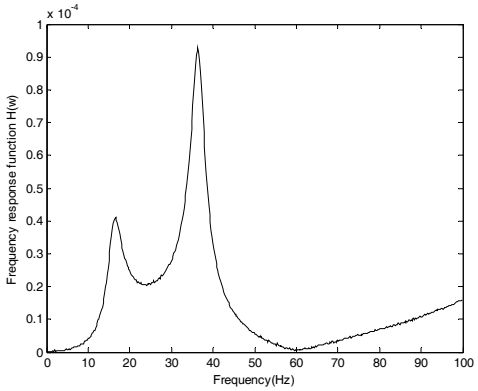

Figure 22. FRF H_{11} at U/Ucr = 0 with 5% noise using traditional inverse method, based on multi-degree-of-freedom model.

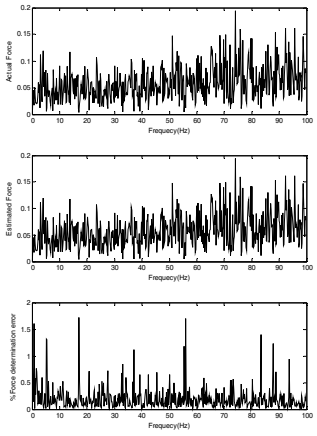

Figure 23. Actual, estimated, translational force and percentage error, U/Ucr = 2/3 with 5% noise using traditional inverse technique, based on multi-degree-of-freedom model.

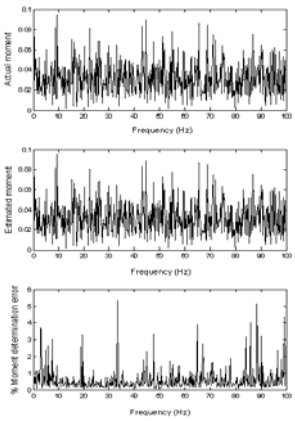

Figure 24. Actual, estimated rotational moment and percentage error, U/Ucr = 2/3 with 5% noise using traditional inverse technique, based on multi-degree-of-freedom model.

Next, the frequency response function H_{11}, actual, estimate forces and moments, as well as percentage errors are calculated by "H_1" and "H_2" methods. The noise is added through Eqns. (13) and (14). The results plotted in following figures are formulated at air speed of 9.34m/s and noise level of 5%. As shown in Figs. 26 and 27, the average percentage errors for force and moment calculated from H_1 method are 17.36% and 15.80%. Nevertheless, the percentage errors given by H_2 method are 22.42% and 20.74%, as displayed in Figs. 29 and 30.

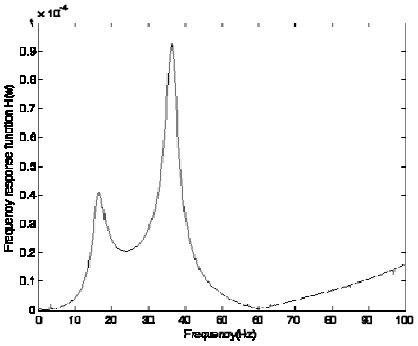

Figure 25. FRF H_{11} at U/Ucr = 0 with 5% noise using H_1 method, based on multi-degree-of-freedom model.

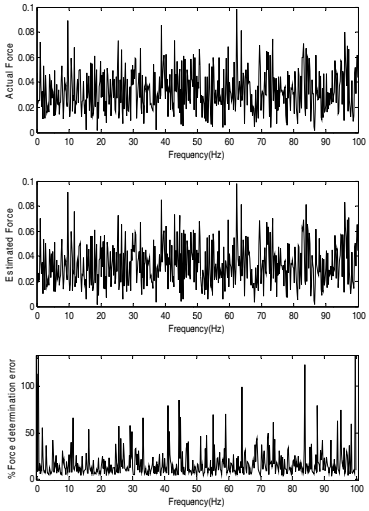

Figure 26. Actual, estimated translational force and percentage error, U/Ucr = 2/3 with 5% noise using H_1 method, based on multi-degree-of-freedom model.

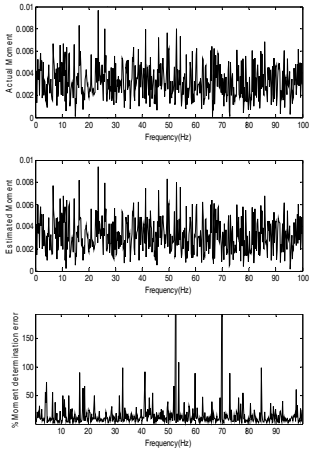

Figure 27. Actual, estimated rotational moment and percentage error, U/Ucr = 2/3 with 5% noise using H_1 method, based on multi-degree-of-freedom model.

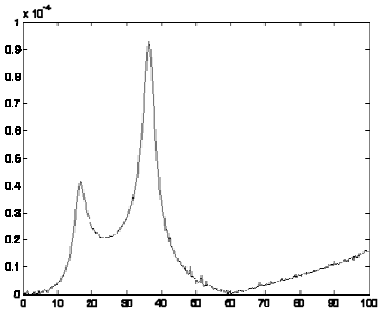

Figure 28. FRF H_{11} at U/Ucr = 0 with 5% noise using H_2 method, based on multi-degree-of-freedom model.

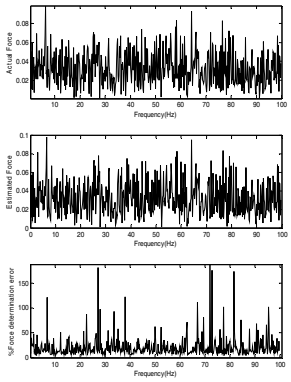

Figure 29. Actual, estimated translational force and percentage error, U/Ucr = 2/3 with 5% noise using H_2 method, based on multi-degree-of-freedom model.

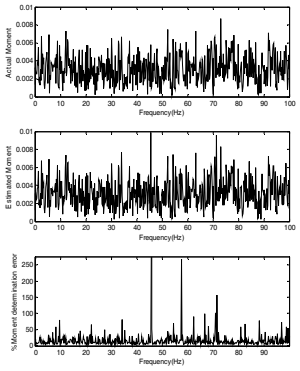

Figure 30. Actual, estimated rotational moment and percentage error, U/Ucr = 2/3 with 5% noise using H_2 method, based on multi-degree-of-freedom model.

Finally, actual, estimated forces and moments, and the percentage errors are recalculated using the "F_1" and "F_2" methods and plotted in Figs. 31 to 34. The displayed results are obtained at the airspeed of 9.34 m/s and noise level of 5%. According to Figs. (31) and (32), the average percentage errors for the force and moment yielded from the "F_1" method are 8.77% and 10.62%, while these values are 14.62% and 15.72% yielded from the "F_2" method, as shown in Figs. (33) and (34).

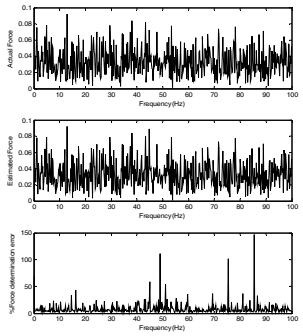

Figure 31. Actual, estimated translational force and percentage error, U/Ucr = 2/3 with 5% noise using F_1 method, based on multi-degree-of-freedom model.

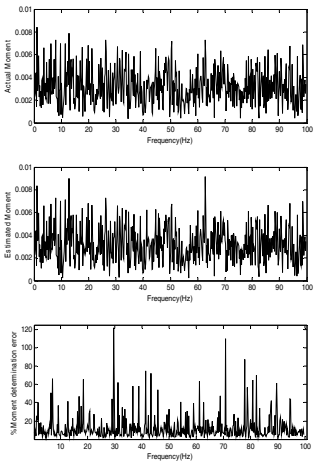

Figure 32. Actual, estimated rotational moment and percentage error, U/Ucr = 2/3 with 5% noise using F_1 method, based on multi-degree-of-freedom model.

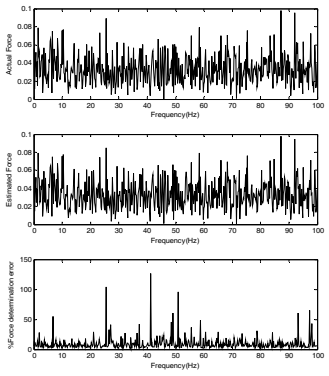

Figure 33. Actual, estimated translational force and percentage error, U/Ucr = 2/3 with 5% noise using F_2 method, based on multi-degree-of-freedom model.

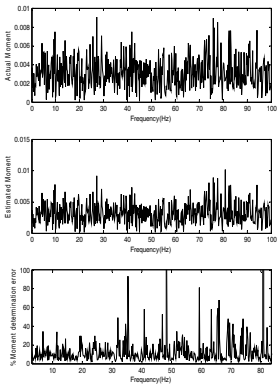

Figure 34. Actual, estimated rotational moment and percentage error, U/Ucr = 2/3 with 5% noise using F_2 method, based on multi-degree-of-freedom model.

8. Discussions

In above sections, the forces and moments estimated from the traditional pseudo-inverse method, "H_1" and "H_2" methods, as well as "F_1" and "F_2" methods are compared to the actual values. From these comparisons, it is found that the errors caused by the pseudo-inverse method are much lower than those errors yielded from other methods, which is because in that method, the mass, stiffness and damping matrices are directly obtained from the two degrees-of-freedom and multi-degree-of-freedom models. However, in reality, those matrices are difficult to be obtained from a real complicated model. In the "H_1", "H_2", "F_1", "F_2" methods which use cross-spectrum and auto-spectrum, the frequency response function is estimated from the input force and the

corresponding structural response. Therefore, such methods are easier to apply for force determination in real problems.

Compared to the "H_1" and "H_2" methods, the "F_1" and "F_2" methods yield lower errors in identifying the force and moment values. This is because the direct determination methods directly calculate the inverted frequency response matrix, therefore eliminate the error introduced during the inversion of the frequency response matrix.

It is also found from our study that when the airspeed and noise level increase, the force determination errors also rise.

9. Conclusions

This paper presents several force determination methods and applies those methods to identify the aerodynamic forces and moments acting on an aircraft wing model during the flight. Two wing models, a two degrees-of-freedom model and a multi-degree-of-freedom model are created and used for this study. The estimated force and moments are compared to the actual values. From the comparisons, it is concluded that with available mass, stiffness, and damping matrices, the traditional pseudo-inverse method provides the best accuracy. However, considering both accuracy and applicability, the direct determination methods "F_1" and "F_2" are recommended for such problem. Also, the accuracy of the created two degrees-of-freedom and multi-degree-of-freedom wing models are verified through this study. The results obtained from this study are ready to be further verified through a series of real experiments.

References

[1] R. M. Kirby, Z. Yosibash, G.E. Karniadakis, "Towards stable coupling methods for high order discretization of fluid-structure interaction: Algorithms and observations", *Journal of Computational Physics*, 223 (2), 2007, 489-518.

[2] F. Liu, J. Cai, Y. Zhu, H.M. Tsai, A.S.F. Wong, "Calculation of wing flutter by a coupled fluid-structure method", *Journal of Aircraft*, 38 (2), 2001, 334-342.

[3] J. A. Fabunmi, "Effects of structural modes on vibratory force determination by the pseudoinverse technique", *AIAA Journal*, 24 (3), 1986, 504-509.

[4] R. Kamakoti, Y. Lian, S. Regisford, A. Kurdila, W. Shyy, *Computational aeroelasticity using a pressure-based solver*, AIAA-2002-869, AIAA Aerospace Sciences Meeting and Exhibit, 40th, Reno, NV, Jan. 14-17, 2002.

[5] Y. Liu, W.S. Shepard, Jr., "Dynamic force identification based on enhanced least squares and total least-squares schemes in the frequency domain", *Journal of Sound and Vibration*, 282(1/2), 2005, 37-60.

[6] E. Parloo, P. Verboven, P. Guillaume, M.V. Overmeire, "Force identification by means of in-operation modal models", *Journal of Sound and Vibration*, 262 (1), 2003, 161-173.

[7] I. Lee, S.-H. Kim, "Aeroelastic analysis of a flexible control surface with structural nonlinearity", *Journal of Aircraft*, 32(4), 1995, 868-874.

[8] S. -H. Kim, I. Lee, "Aeroelastic analysis of a flexible airfoil with a freeplay nonlinearity", *Journal of Sound and Vibration*, 193 (4), 1996, 823-846.

[9] B. H. K. Lee, S.J. Price, Y.S. Wong, "Nonlinear aeroelastic analysis of airfoils: bifurcation and chaos", *Progress in Aerospace Sciences*, 35 (3), 1999, 205-334.

[10] I. D. Roy, W. Eversman, "Adaptive flutter suppression of an unswept wing", *Journal of Aircraft*, 33 (4), 1996, 775-783

[11] W. Eversman, I.D. Roy, "Adaptive flutter suppression using multi-input/multi-output adaptive least mean square control", *Journal of Aircraft*, 34 (2), 1997, 244-250.

[12] G. Dimitriadis, J. E. Cooper, "A method for identification of non-linear multi-degree-of-freedom systems", *Proceedings of the Institution of Mechanical Engineers, Part G: Journal of Aerospace Engineering*, 212 (4), 1998, 287-298.